

Impact of Calcium Store Overload and Electrical Dynamics on Cardiac Myocytes

REU Site: Interdisciplinary Program in High Performance Computing

Amanda M. Alexander¹, Erin K. DeNardo², Eric Frazier III³,
Michael McCauley⁴, Nicholas Rojina⁵
Graduate assistant: Zana Coulibaly⁴

Faculty mentor: Bradford E. Peercy⁴, Client: Leighton T. Izu⁶

¹Department of Mathematics, Western Washington University

²Department of Electrical and Systems Engineering, Washington University in St. Louis,

³Department of Mathematics and Computer Science, La Salle University,

⁴Department of Mathematics and Statistics, UMBC,

⁵Department of Mathematics, University of North Carolina, Chapel Hill,

⁶Department of Pharmacology, University of California, Davis

Technical Report HPCF-2015-25, hpcf.umbc.edu > Publications

1 Introduction

The heart's main function of pumping blood to the body is a complicated process separated into two major steps. Initially, the heart is relaxed and blood flows freely into the ventricles and atria from the veins, then the atria contracts and pumps more blood to the ventricles. The atria relaxes and the inlet valves between these and the ventricles close, producing the initial thump of the heartbeat, as pressure builds while the ventricles contract. This pressure also forces the outlet valves open, allowing blood to flow into the arteries and aorta. As the ventricles relax, the outlet valves then close, producing the second thump of the heartbeat. Once the atria and ventricles are relaxed, the inlet valves reopen, allowing the compartments to fill with blood again as the process repeats.

If the heart's contractile abilities are impaired in any way, the rest of the body cannot perform properly. Despite advances in cardiology research, cardiac arrhythmia remains an influential cause of morbidity and mortality in the United States [1]. Recent advances involve the application of devices, such as pacemakers or defibrillators, and the outlook of antiarrhythmic drug therapy up to this point is grim [21], so it is necessary to understand how some pathological conditions within cardiac myocytes can lead to dysfunction of these cells. Calcium mishandling can play a major role in disruption of overall cardiac function by preventing the ability of the heart muscles to relax between heartbeats and thus impair their pumping blood to the body [12].

2 Background

The sarcoplasmic reticulum (SR) is the main Ca^{2+} storage organelle within cardiac myocytes. Local Ca^{2+} releases in cardiac myocytes are known as calcium sparks, and they are required for cardiac muscle contraction; these are elementary events that trigger calcium waves. [5].

Ca²⁺ release units (CRUs) act as calcium-sensitive channels between the SR and the intracellular space of the cell, and they are the pathway by which spark releases are made from the SR. The level of contractions of the heart are directly related to elevated Ca²⁺ levels, so an inability of cytosolic calcium to diffuse and be effectively removed from the cell impairs the ability of cardiomyocytes to relax. The propagation of waves occur due to the process of Ca²⁺-induced-Ca²⁺-release (CICR) [7] whereby the elevated level of Ca²⁺ in the extracellular space triggers CRUs to fire and release additional Ca²⁺. The Ca²⁺ moving into the intracellular space then acts as a messenger, activating contraction by increasing the concentration of cytosolic Ca²⁺ and therefore directly activating CICR and release of Ca²⁺ from the SR [4].

Spontaneous Ca²⁺ waves are typically observed during overload of Ca²⁺ concentration in the SR, causing depolarization of the cell membrane. Afterdepolarizations occur when oscillations in membrane potential depolarize the cell membrane to its threshold potential, inducing a spontaneous action potential [1]. Ca²⁺ channels activate on membrane depolarization and respond to action potentials. These channels are responsible for converting the electrical signal provided by the action potential to the movement of Ca²⁺ into the cell.

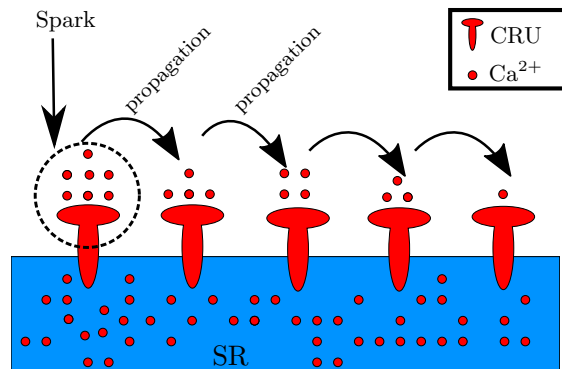


Figure 2.1: Triggering of Ca²⁺ waves

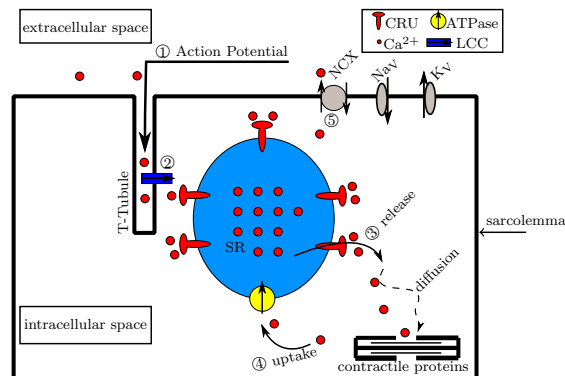


Figure 2.2: Diagram of cellular space

Extracellular calcium (Ca²⁺) ions are necessary for contraction to occur in cardiac muscle cells [16]. Inward flow of a Ca²⁺ current is important in linking electrical and mechanical excitation in the cardiac muscle cells. The L-type calcium channel (LCC) in the plasma membrane, connecting the extracellular to the intracellular space, is responsible for the excitation-contraction coupling (ECC), the physiological process by which the electrical stimulus in the form of an action potential is converted to a mechanical response, the contraction of the heart [2].

SR Ca²⁺ release contributes the majority of Ca²⁺ for cytosolic contractile activation, and SR load critically regulates SR Ca²⁺ release during both ECC and spontaneous SR Ca²⁺ release. These conditions have the ability to cause delayed afterdepolarizations and arrhythmias [14]. Spontaneous Ca²⁺ waves are typically observed during overload of Ca²⁺ in the SR, causing depolarization of the cell membrane. Certain conditions allow the cell to reach the threshold for activation of spontaneous electrical activity. This occurs due to the induction of inward current by the Ca²⁺ waves produced.

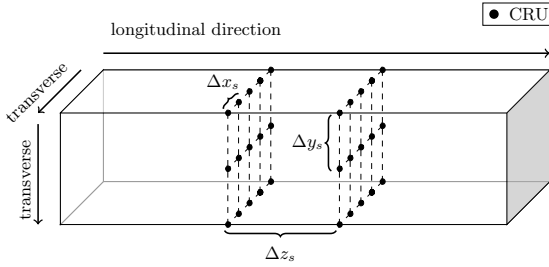
Ca²⁺ buffering is a control system so as to slow down or regulate certain intracellular

processes. It is the rapid binding of Ca^{2+} to other substances in a space in the cell. When the Ca^{2+} binds to buffers in order to form another compound, there is then a lower free Ca^{2+} concentration in the SR [8]. Calsequestrin is non-mobile and acts as a major buffer in cardiac muscle cells by lowering the amount of unbound Ca^{2+} in the SR space [11].

In this paper, we present a mathematical model for studying certain conditions in the myocytes in order to determine their role in resulting Ca^{2+} waves. Key elements to the model are the incorporation of the SR Ca^{2+} store and its Ca^{2+} flux through CRUs into the cell, buffer species in the SR, and a voltage model for current differences across the membrane so as to incorporate incoming Ca^{2+} from the extracellular space through LCCs.

3 Methodology

Since our model will use partial differential equations, we apply the finite element method (FEM) in order to solve over a specific time period. FEM is a method of approximation used to solve systems of partial differential or nonlinear equations over complicated domains such as in Figure 3.1. Using a computer-based model, we are able to compute a finite element matrix and vector.



Due to the complex nature of the surface of a cardiac myocyte (Figure 2), the cell is modeled as a rectangular prism with CRU's in a lattice structure to emulate their role as point sources of Ca^{2+} .

Figure 3.1: Our PDE domain

In order to track the change in concentrations of calcium and buffer species in the cytosol, we utilize the following system of partial differential equations:

$$\frac{\partial c}{\partial t} = \nabla \cdot (D_c \nabla c) + \sum_{i=1}^{nsc} R_i + J_{\text{CRU}} + J_{\text{leak}} - J_{\text{pump}}, \quad (3.1)$$

$$\frac{\partial b_i}{\partial t} = \nabla \cdot (D_{b_i} \nabla b_i) + R_i, \quad (3.2)$$

$$R_i = -k_i^+ c b_i + k_i^- (b_{iT} - b_i). \quad (3.3)$$

Equation 3.1 represents the change in calcium concentration over time, c , equation 3.2 represents the change in each buffer species concentration over time, b_i , and equation 3.3 represents the reaction of buffer species with calcium as it relates to both their concentrations. As equation 3.2 will be self-explanatory knowing equation 3.1, we focus on explaining equation 3.1 first. The first term, $\nabla \cdot (D_c \nabla c)$, is the diffusion of Ca^{2+} with diffusion coefficient matrix, D , multiplied by the gradient vector of c , of which the gradient vector is then taken. The second term, $\sum_{i=1}^{n.s} R_i$, is the sum of the reaction terms when each buffer species reacts with

calcium, allowing us to keep track of the calcium changes due to these reactions. The third term, J_{CRU} , represents the influx of calcium when the CRU opens. The fourth term, J_{leak} , represents the leak of calcium from the SR into the cytosol that keeps the cell at equilibrium during basal level. The fifth term, J_{pump} represents the pumping of calcium into the SR. The mathematical equations representing these “ J ” terms are below:

$$J_{pump} = V_{pump} \frac{c^{n_{pump}}}{K_{pump}^{n_{pump}} + c^{n_{pump}}}, \quad (3.4)$$

$$J_{leak} = V_{pump} \frac{c_0^{n_{pump}}}{K_{pump}^{n_{pump}} + c_0^{n_{pump}}}, \quad (3.5)$$

$$J_{CRU} = \sum \hat{\sigma} \mathcal{O}(c, t) \delta(X - X_i), \quad (3.6)$$

$$\mathcal{O}(c, t) = \begin{cases} 1 & \text{if } \alpha \leq J_{prob} \\ 0 & \text{if } \alpha > J_{prob} \end{cases}, \quad (3.7)$$

$$J_{prob} = P_{max} \frac{c^{n_{prob}}}{K_{probe}^{n_{prob}} + c^{n_{prob}}}. \quad (3.8)$$

Equations 3.4 and 3.5 are set up so that J_{pump} and J_{leak} balance each other when the calcium concentration is at basal level (i.e. no calcium from CRU’s), but equation 3.4 can also balance out equation 3.6 when there is an increase in calcium due to CRU’s opening. Equation 3.6 is comprised of three terms describing how much, when, and where calcium is released by the CRU. The first term represents how much calcium is released by the CRU, with $\hat{\sigma}$ being the constant maximum release rate of c into the cytosol. The second term is equation 3.7, the gating function, which is 0 if the CRU is closed and 1 if the CRU is open. To determine whether the CRU is open or closed, equation 3.8 calculates this probability based on calcium concentration and other constants determined from experimental data. This J_{prob} value is then compared to a random number α to determine if the CRU opens or stays closed. The third term $\delta(X - X_i)$ is used to model the CRU’s as point sources of calcium in three dimensions, so that calcium is released at just X_i in our model. Like the table below, there will be a table at the end of each subsection defining the parameters used.

Parameters	Definition	Values/Units	Source
n_{sc}	number of cytosol Ca^{2+} buffer species	2	[9]
b_i	cytosol buffer concentrations	50,123 μM	[9]
b_j	SR buffer concentrations	6000 μM	[3]
D_{b_i}, D_{b_j}	cytosol, SR buffer diffusion coefficient matrix	diag(0.0,0.0,0.0) $\mu\text{m}^2/\text{ms}$	[3], [18]
V_{pump}	max. pump rate	2-6 $\mu\text{M}/\text{ms}$	[6]
c_0	initial cytosol calcium concentration	0.1 μM	[9]
X_i	three dimensional vector for CRU location	μm	
$\hat{\sigma}$	maximum rate of release	100-200 $\mu\text{M}\mu\text{m}^3/\text{ms}$	[6]
K_{probe}	sensitivity of CRU to cytosol calcium	5-15 $\mu\text{M}/\text{ms}$	[10]

Table 3.1

3.1 SR Calcium

To improve this current model, we first noticed that SR calcium is not considered in our model, and it is well known that SR calcium concentration has a significant influence on calcium release of the CRUs within a cardiac cell. Therefore, we added it and its buffers to the model by partial differential equations as shown below:

$$\frac{\partial s}{\partial t} = \nabla \cdot (D_s \nabla s) + \sum_{j=1}^{nss} R_j - \gamma(J_{CRU} + J_{leak} - J_{pump}), \quad (3.9)$$

$$\frac{\partial b_j}{\partial t} = \nabla \cdot (D_{b_j} \nabla b_j) + R_j. \quad (3.10)$$

Similar to calcium in the current model, equation 3.9 is the change in SR calcium concentration, s , over time with many of the same variables. However, notice that the signs of all the “J” terms are the opposite of what they were in equation 3.1 since whenever c increases, s decreases. Also note that γ represents the ratio of the volume of the cytosol to the volume of the SR to make the change in concentration of the SR account for its significantly smaller volume. For clarity, notice that the summing of reaction terms is changed to R_j to represent SR buffers, b_j . Now to actually have s influence CRU openings, we had to modify J_{CRU} and some of its terms as in the following:

$$J_{CRU} = \sum (\hat{\sigma} \frac{s - c}{s_0 - c_0}) \mathcal{O}(c, s, t) \delta(X - X_i), \quad (3.11)$$

$$J_{prob} = P_{max} \frac{c^{n_{prob}}}{K_{prob_c}^{n_{prob}} + c^{n_{prob}}} \cdot \frac{s^{n_{prob}}}{K_{prob_s}^{n_{prob}} + s^{n_{prob}}}. \quad (3.12)$$

Notice that in equation 3.11, there is change in the first term $\hat{\sigma}$ from being a constant maximum release rate to being affected by the concentrations of s and c with the fraction $(s - c)/(s_0 - c_0)$ ranging from 0-1 to act as a scaling factor since $\hat{\sigma}$ isn't necessarily always maximized. The second term is equation 3.7, the gating function, which now has s as an input variable due to the extra term in equation 3.12. This extra term makes J_{prob} depend on SR calcium in such a way that when s is high the probability of the CRU opening is the same as it used to be but s is low the probability of the CRU opening is much smaller.

Parameters	Definition	Values/Units	Source
s_0	initial SR calcium concentration	1,000-10,000 μM	[3], [20]
nss	number of SR Ca^{2+} buffer species	1	
γ	ratio of volume of cytosol to SR	14	[15]
K_{prob_s}	sensitivity of CRU to open due to SR calcium	200,550 $\mu\text{M}/\text{ms}$	

Table 3.2

3.2 Voltage Model

In order to make the model more comprehensive and biologically relevant, we introduced the Morris-Lecar voltage model, described below.

3.2.1 Morris-Lecar Model

A simple conductance model exists in the cardiomyocytes, as described in the model of a barnacle muscle fiber composed of voltage-dependent Ca^{2+} and K^+ channels. In this case, we assume linearity of the instantaneous voltage-current flowing through these channels. The introduction of stimuli produce depolarizations across the cell membrane. Oscillations then begin to occur once the voltage reaches a certain threshold that is imposed by the model. Although external calcium concentration is particularly influential on the nature of the oscillatory behavior, oscillations only occur when both Ca^{2+} and K^+ currents are present and activated at the same time. Thus, the equation below for monitoring voltage has K^+ terms involved. In the same fashion as Morris and Lecar [13], we make use of the different relaxation times of the Ca^{2+} and K^+ conductances to study the oscillating state in some generality as shown below. We have also τ as a scaling factor for the Morris-Lecar model to adjust the action potential duration to fit our model.

$$\frac{\partial c}{\partial t} = \nabla \cdot (D_c \nabla c) + \sum_{i=1}^{nsc} R_i + (J_{CRU} + J_{leak} - J_{pump}) + J_{LCC} + J_{mleak} - J_{mpump}, \quad (3.13)$$

$$\frac{\partial V}{\partial t} = \tau \cdot \frac{1}{C} (I_{app} - g_L(V - V_L) - g_{Ca} m_\infty (V - V_{Ca}) - g_K n (V - V_K)), \quad (3.14)$$

$$\frac{\partial n}{\partial t} = \tau \cdot \lambda_n(V) [n_\infty(V) - n]. \quad (3.15)$$

We study this reduced set of equations, in which the Ca^{2+} system is assumed to be so much faster than the K^+ system that g_{Ca} is instantaneously in steady state at all times [13]. Now we see the effects of voltage on calcium dynamics through the J_{LCC} term and its related “ J ” terms, which are formulated to mirror the J_{pump} and J_{leak} terms from equations 3.4, 3.5.

$$J_{LCC} = \kappa \cdot \frac{S \cdot g_{Ca} m_\infty (V - V_{Ca})}{2F}, \quad (3.16)$$

$$J_{mleak} = \frac{c_0^{mn_{pump}}}{K_{mpump}^{mn_{pump}} + c_0^{mn_{pump}}} \quad (3.17)$$

$$J_{mpump} = \frac{c^{mn_{pump}}}{K_{mpump}^{mn_{pump}} + c^{mn_{pump}}} \quad (3.18)$$

Note that, due to a lack of evidence on the actual location of LCC channels, we have implemented two versions of our voltage model: one where Ca^{2+} flux from the LCC channels is only present across from the CRUs of the SR and one where Ca^{2+} flux from the LCC channels is present around the entire plasma membrane. In the same manner as (CRUs are assumed to release the same average amount of Ca^{2+}), LCCs are assumed to release the same average amount of Ca^{2+} as well. Thus while the total amount of Ca^{2+} influx from voltage is the same regardless of which version of the model we use, when we assume Ca^{2+} flux from the LCC channels due to voltage is only present across from the CRUs of the SR we make use of the dirac delta function to model the LCC channels as point sources. However, this

causes a change in units we must account for as shown below:

$$J_{LCC}^{CRUs} = J_{LCC}^{everywhere} \quad (3.19)$$

$$\frac{1}{\Omega} \int J_{LCC}^{CRUs} d\Omega = \frac{1}{\Omega} \int J_{LCC}^{everywhere} d\Omega \quad (3.20)$$

$$\int \sum_{i=1}^{6975} J_{LCC}^{CRUs} \cdot \delta(X - X_i) d\Omega = \int J_{LCC}^{everywhere} d\Omega \quad (3.21)$$

$$\sum_{i=1}^{6975} J_{LCC}^{CRUs} = J_{LCC}^{everywhere} \cdot |\Omega| \quad (3.22)$$

$$6975 \cdot J_{LCC}^{CRUs} = J_{LCC}^{everywhere} \cdot |\Omega| \quad (3.23)$$

$$J_{LCC}^{CRUs} = J_{LCC}^{everywhere} \cdot \frac{|\Omega|}{6975} \quad (3.24)$$

In order to account for this difference, we multiply our J_{LCC} term by volume/(number of CRUs) = $(12.8 \cdot 12.8 \cdot 64)/6975 = 1.503$ when we assume LCC channels are around the entire plasma membrane.

Equation 3.14, combined with the parameters below, represents a nonlinear Hodgkin-Huxley-like equation, and explains the excitation of the cell by varying voltage in the cell, with assigned constants from experimental data.

$$m_{\infty}(V) = \frac{1}{2} \left[1 + \tanh \left(\frac{V - V_1}{V_2} \right) \right] \quad (3.25)$$

$$n_{\infty}(V) = \frac{1}{2} \left[1 + \tanh \left(\frac{V - V_3}{V_4} \right) \right] \quad (3.26)$$

$$\lambda_n(V) = \bar{\lambda}_n \cosh \left(\frac{V - V_3}{2V_4} \right) \quad (3.27)$$

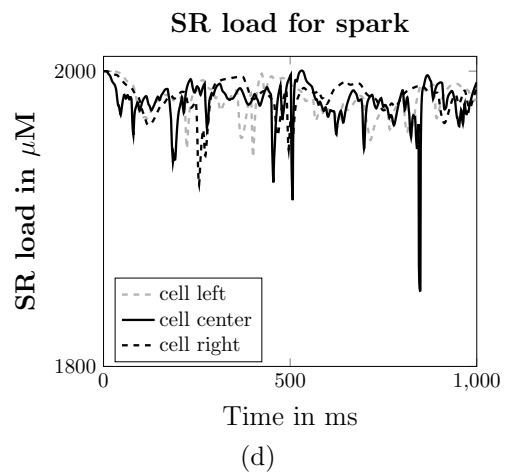
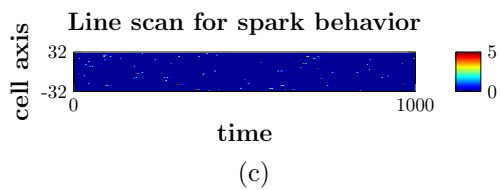
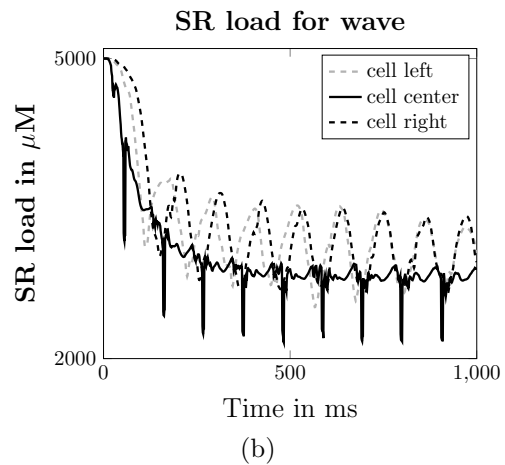
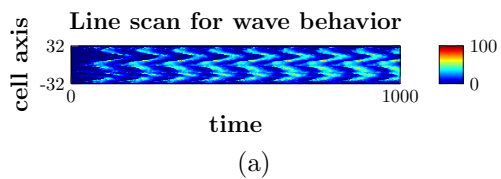
Parameters	Definition	Values/Units	Source
I	applied current	$10 \mu\text{A}/\text{cm}^2$	[13]
C	membrane capacitance	$20 \mu\text{F}/\text{cm}^2$	[13]
g_L	max./instantaneous conductance for leak	$2 \text{mmho}/\text{cm}^2$	[13]
g_{Ca}	max./instantaneous conductance for Ca^{2+}	$4 \text{mmho}/\text{cm}^2$	[13]
g_K	max./instantaneous conductance for K^+	$8 \text{mmho}/\text{cm}^2$	[13]
V_L	equilibrium potential for leak conductance	-50 mV	[13]
V_{Ca}	equilibrium potential for Ca^{2+} conductance	100 mV	[13]
V_K	equilibrium potential for K^+ conductance	-70 mV	[13]
λ_n	max. rate constant for K^+ channel opening	s^{-1}	[13]
S	surface area of the cell	$3604.48 \mu\text{m}^2$	[9]
mn_{pump}	for plasma membrane, similar to hill coefficient	2	
K_{mpump}	similar to Ca^{2+} sensitivity parameter	0.18	
V_1	potential at which $M_\infty = 0.5$	-1 mV	[13]
V_2	reciprocal of slope of voltage dependence of M_∞	15 mV	[13]
V_3	potential at which $N_\infty = 0.5$	10 mV	[13]
V_4	reciprocal of slope of voltage dependence of N_∞	4.5 mV	[13]
τ	scaling factor of Morris-Lecar model to fit AP duration	$0.1 \mu\text{M} \mu\text{m}^3/\text{ms}$	
κ	scaling factor of J_{LCC}	0.01	

Table 3.3

4 Results

In order to visualize the data sets produced by our model, we utilize Matlab code to make three different types of images: line-scans, SR plots, and voltage/flux plots. For the line-scan, cytosol Ca^{2+} concentration (μM) is tracked along the center of the cell in the longitudinal direction at each millisecond, and then space is graphed vertically and time horizontally. The final image is colored based off of Ca^{2+} concentration from 0 to $5\mu\text{M}$; red indicates high concentration and blue indicates low concentration. SR plots track SR Ca^{2+} concentration ($\mu\text{M}/\text{ms}$), c , along three different lines, left, center, and right, within the SR. Voltage/flux plots show the voltage across the cell membrane (mV) and Ca^{2+} flux ($\mu\text{M}/\text{ms}$) through the LCC channels at each millisecond, and overlay their graphs.

Based on our various additions to the model in the C code, we were able to produce numerous results indicating various types of Ca^{2+} dynamics. These results were grouped into three major behaviors: localized sparks, waves, or blowups. The images in Figure 4.1 depict an example line-scan image of each behavior type.



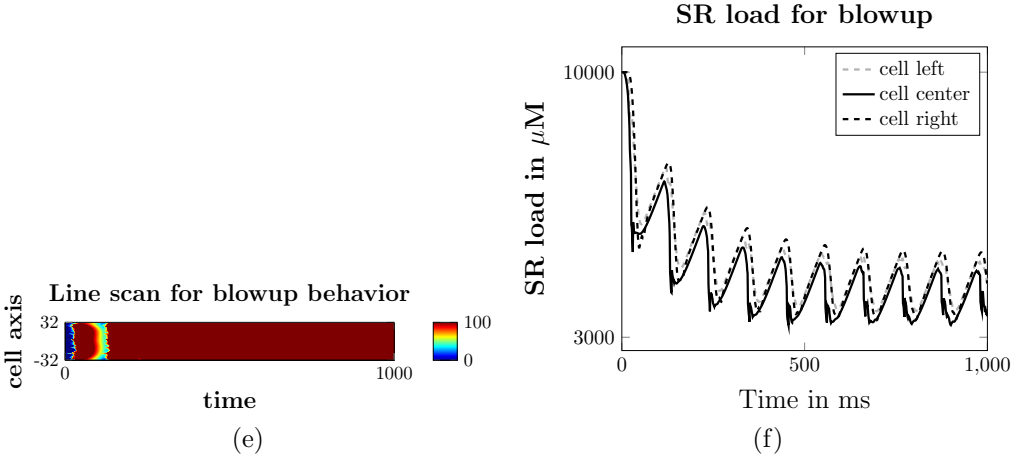


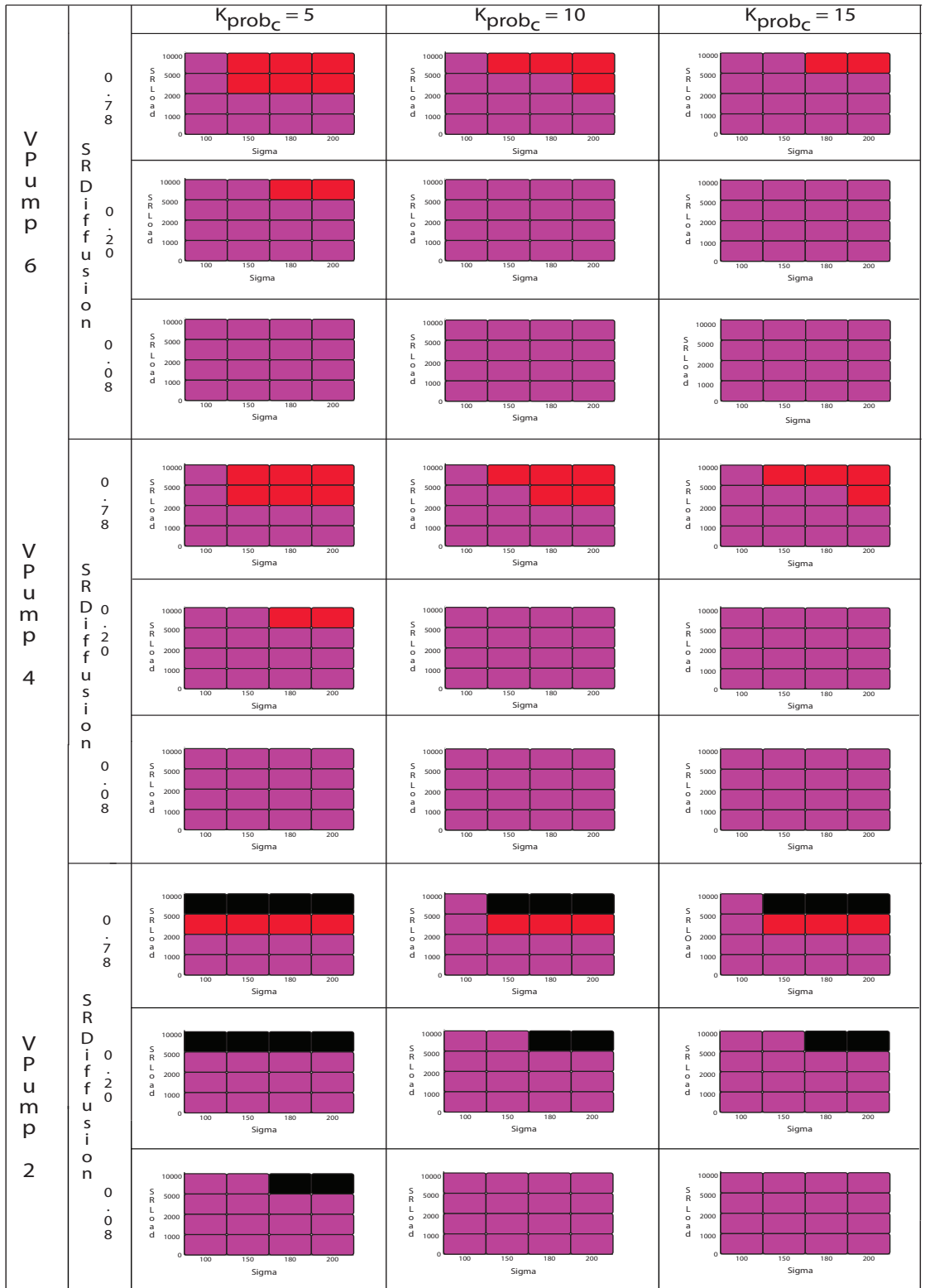
Figure 4.1: (a),(b) Varied Parameters: $\hat{\sigma} = 150 \mu\text{M}\mu\text{m}^3/\text{ms}$, $s_0 = 5000 \mu\text{M}$, $K_{prob_c} = 10 \mu\text{M}$
(c),(d) Varied Parameters: $\hat{\sigma} = 200 \mu\text{M}\mu\text{m}^3/\text{ms}$, $s_0 = 2000 \mu\text{M}$, $K_{prob_c} = 15 \mu\text{M}$
(e),(f) Varied Parameters: $\hat{\sigma} = 200 \mu\text{M}\mu\text{m}^3/\text{ms}$, $s_0 = 10000 \mu\text{M}$, $K_{prob_c} = 5 \mu\text{M}$

Note that in Figure 4.1a there is an almost periodic sideways “V” shape to the lighter blue shades where Ca^{2+} concentration in the cytosol is higher in the cell. The farthest left point of a V implies Ca^{2+} release from minimal CRUs in the middle of the cell, triggering Ca^{2+} release at nearby CRUs which also trigger Ca^{2+} release at nearby CRUs to them. This CICR moves farther and farther towards the end of the cell, in effect creating what we call a wave of Ca^{2+} release. This Ca^{2+} release is reflected in Figure 4.1b, the corresponding graph of SR Ca^{2+} load over time. The downward spikes of the SR load correspond to the Ca^{2+} increase in the cytosol at the same time. Also, note that, in the SR load, there is much more fluctuation at the edges of the SR as these are where the CRUs are located. Despite this decrease in SR load, however, the scale on the left, indicating SR load (μM) shows that the decreasing Ca^{2+} concentration stabilizes at about $\sim 3000 \mu\text{M}$.

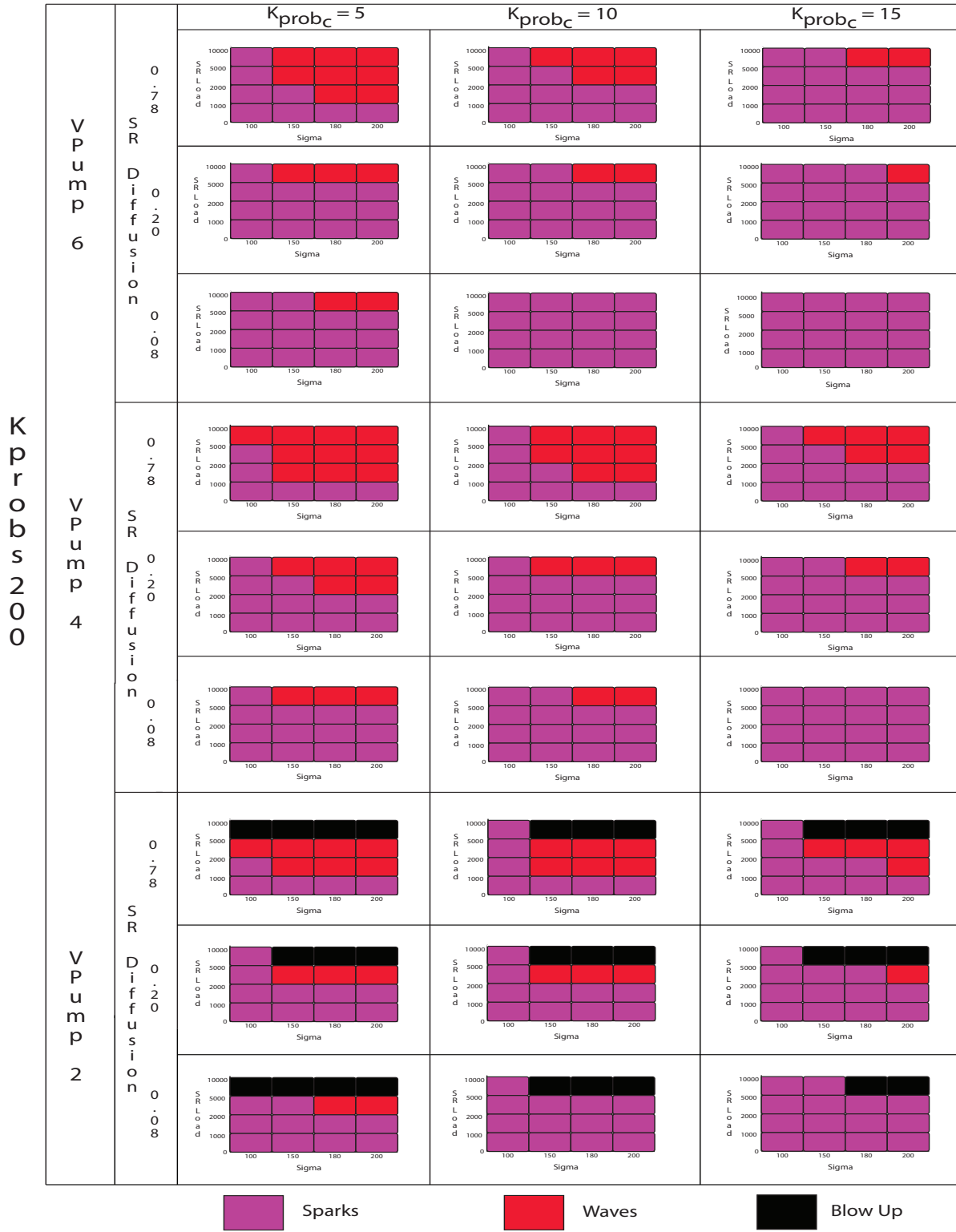
Figure 4.1c shows small, spontaneous releases of Ca^{2+} over time. These are known as sparks because, although calcium was released, CICR-triggered wave propagation did not occur. In the corresponding SR plot, Figure 4.1d, the downward spikes in SR again correspond to small increases in Ca^{2+} concentration in the cytosol. Take note, as well, that the scaling of Figure 4.1c, the scale for concentration levels has a smaller range than that of Figure 4.1a and 4.1e, as the concentration increases during spark dynamics are much more minimal, and this explains why no further sparks, and thus no CICR, is triggered.

Figure 4.1e shows a quick, massive increase in Ca^{2+} in the cytosol that is never recovered back into the SR. This is what we call a blowup, because Ca^{2+} floods the cytosol and the pumps to the SR and extracellular space cannot act quickly enough in order to remove it. Figure 4.1f shows this failure to pump Ca^{2+} back into the SR with its dramatic decrease in SR Ca^{2+} load over time, as depicted on the left scale, with a decrease to about 30% of the starting concentration.

Kprob_c 550



(a)



(b)

Figure 4.2: SR without buffers

After we implemented the SR and its buffers into the model, we wanted to compare calcium dynamics with and without buffers in the SR as we changed certain parameters. Figures 4.2 and 4.3 represent the different parameter sets we chose to fill in the values for K_{prob_c} , $\hat{\sigma}$, SR calcium load, s_0 , diffusion coefficient, D_{SR} , and K_{prob_s} , each found from researching cardiac cells of different animals. Every small colored square represents one simulation. Each parameter had multiple values, K_{prob_c} in $\{5, 10, 15\}\mu\text{M}/\text{ms}$, $\hat{\sigma}$ in $\{100, 150, 180, 200\}\mu\text{M}\mu\text{m}^3/\text{ms}$, s_0 in $\{1000, 2000, 5000, 10000\}\mu\text{M}$, diffusion coefficient in $\{0.08, 0.20, 0.78\}\mu\text{m}^2/\text{ms}$, V_{pump} in $\{2, 4, 6\}\mu\text{M}/\text{ms}$, and K_{prob_s} in $\{200, 550\}\mu\text{M}/\text{ms}$.

Figure 4.4 below shows how we use τ to make the oscillations of the voltage match the timing of the action potential and how we use κ to scale the flux appropriately. Figure 4.5 contrasts a line-scan from a run assuming that LCCs are everywhere in the cell membrane, Figure 4.5a, to a line-scan from a run assuming that LCCs are found only near CRUs, 4.5c. Figure 4.5 also contrasts an SR plot with the LCCs everywhere in the cellular membrane, Figure 4.5a, to an SR plot with the LCCs only near CRUs, Figure 4.5c. In order to preserve the same overall calcium flux through the cell membrane for every simulation, flux through each LCC in the model assuming that LCCs are everywhere will be less than that of the LCCs in the CRU-limited model, as shown in Figure 4.4.

Kprob_c 550



(a)

K prob_c 200



(b)

Figure 4.3: SR with buffers

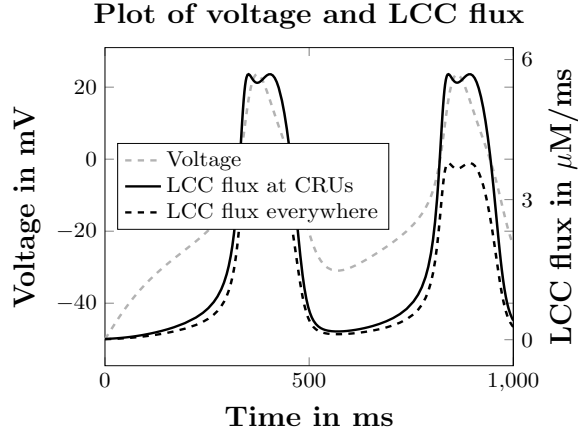


Figure 4.4

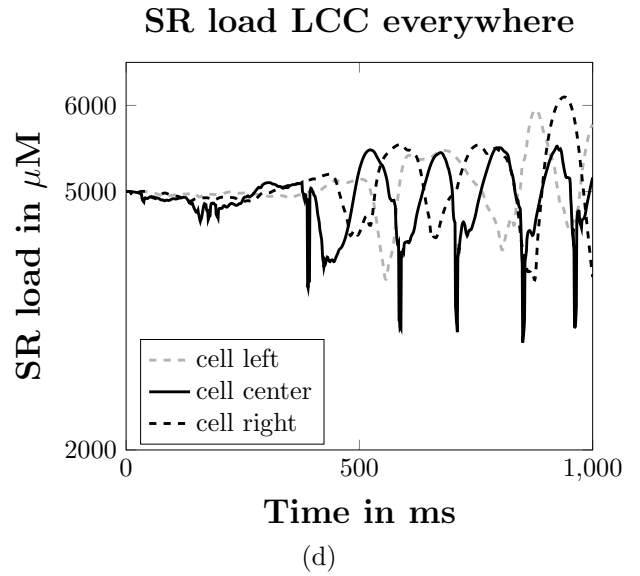
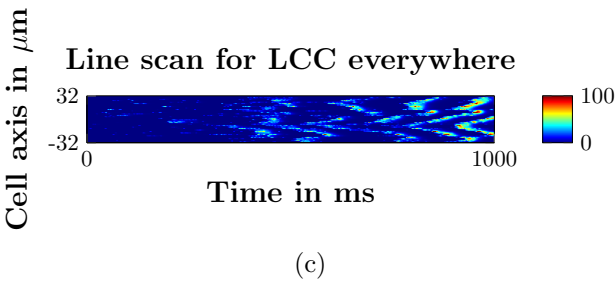
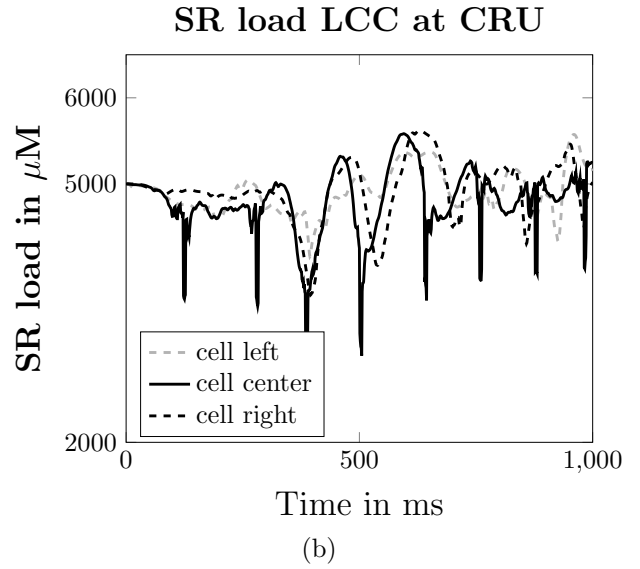
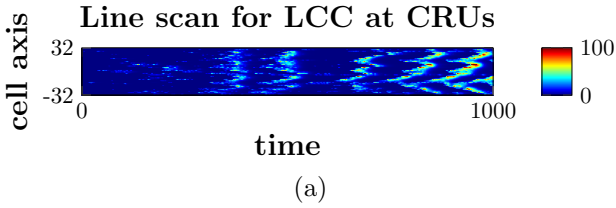


Figure 4.5: Parameters for all diagrams:

$$\hat{\sigma} = 150 \mu\text{M}\mu\text{m}^3/\text{ms}, s_0 = 5000 \mu\text{M}, K_{probe} = 10 \mu\text{M}, D_{SR} = 0.78 \mu\text{m}^2/\text{ms}, V_{pump} = 4 \mu\text{M}/\text{ms}$$

5 Discussion

5.1 SR Calcium Load

After including the effects of a dynamic SR calcium concentration in the mathematical model and adapting the given equations 3.11 and 3.12, we observed, through line-scan images similar to those in Figure 4.1, the resulting Ca^{2+} dynamics. The result types are given with $K_{prob_s} = 550$ in Figure 4.2a and $K_{prob_s} = 200$ in Figure 4.2b.

As evidenced from the comparison of Figures 4.2a and 4.2b, when K_{prob_s} was decreased, the production of waves became more likely. This trend makes sense within the biological model, as K_{prob_s} signifies the CRU sensitivity to SR Ca^{2+} concentration, so a lower sensitivity value means that the CRU will be more likely to open and allow Ca^{2+} to enter into the cytosol, because it has a lower Ca^{2+} concentration at which it opens. Similarly to the CRU sensitivity to SR Ca^{2+} , when K_{prob_c} , the CRU sensitivity to cytosolic Ca^{2+} , increases, waves occur less often. This also aligns with the biological model, as the CRUs are less likely to open until higher concentrations of cytosolic Ca^{2+} are reached.

When V_{pump} is increased, waves occur less under conditions that are otherwise the same. This also aligns with the biological phenomena. Since V_{pump} is the strength of the pump that pulls Ca^{2+} back into the SR, a higher value will mean that the Ca^{2+} is taken back more quickly into the SR and then is not available to trigger other CRUs to spark.

Increasing D_s brought about waves more often. Though this seems strange since this diffusion is only of the Ca^{2+} within the SR, if Ca^{2+} moves about more easily within the SR then it may be more likely to reach the CRU and travel through it into the cytosol, thus increasing the cytosolic Ca^{2+} concentration.

Increased s_0 also shows an increased occurrence of waves. This is also in alignment with the biological model, as an increased concentration of Ca^{2+} in the SR at the same K_{prob_s} would cause the CRUs to open and fire more often.

Waves also become more common as $\hat{\sigma}$ increases, aligning with intuition based upon the biological background. As the maximum release rate through the CRUs increases, then more Ca^{2+} will flow into the intracellular space per unit time.

When the SR was loaded with high Ca^{2+} concentration ($s_0 = 10000 \mu\text{M}$) and high SR diffusion coefficient ($D_s = 0.78 \mu\text{m}^2/\text{ms}$) at low strength of the SR pump ($V_{pump} = 2 \mu\text{M}/\text{ms}$), the cytosol floods with Ca^{2+} to the point where the pump, since it is so weak, is unable to respond properly. At these high concentrations, when $\hat{\sigma}$ is a higher value, since the rate by which Ca^{2+} leaves the SR and enters the intracellular space is higher, the cell will present a similar inability to recover from these high concentrations of Ca^{2+} .

5.2 SR Buffers

Upon including a buffer species, particularly calsequestrin, in the SR, the simulation results given in Figures 4.3a and 4.3b have less wave occurrences and less blow-outs under the conditions specified in Section 5.1, compared to those from simulations run before including an SR buffer (Figures 4.2a and 4.2b).

Since SR buffers decrease the concentration of SR calcium available to signal CRUs to open (Equation 3.3), we expect the presence of wave dynamics to decrease dramatically.

Keeping the parameters constant, Figures 4.3a and 4.3b show that most runs that produced waves without buffers now show a spark dynamic instead, as predicted. It is surprising, however, to see that almost none of the buffered simulations turn out to have waves, even those which exhibit a major blowup without buffers, as depicted in Figures 4.2a and 4.2b.

5.3 Voltage: Morris-Lecar Model

Having set up two versions of our voltage model, after implementing the Morris-Lecar Model (Section 3.2.1) and looking over our previous simulations, we chose a set of parameters to run that had only produced sparks previously. Since including voltage means that cytosol Ca^{2+} concentration would further increase, this intuitively meant we would be more likely to see waves on this set of parameters. Our first few runs produced voltage/flux plots like Figure 4.4, where τ successfully fit the voltage to the flux at LCCs. After these runs, however, we also quickly realized that, regardless of being at the CRUs or everywhere or what parameters we were changing, every simulation with voltage increased cytosol Ca^{2+} concentration so much that it resulted in a blow-up dynamic.

From there forward, we implemented κ in equation 3.16 in order to counteract the overflow of extracellular calcium into the cell. With the inclusion of this parameter, and with increased J_{mpump} , we were able to manipulate the simulation to produce some wave-like behavior as shown in Figures 4.5c, 4.5a. Note that, in these figures, we again see cytosol Ca^{2+} concentration increasing at the same time as SR Ca^{2+} concentration decrease. Now, though, these also correspond with a voltage spike. We also see that SR Ca^{2+} concentration fluctuates about the initial concentration.

Considering the use of the same pump sensitivity parameter, in comparing the images in Figure 4.5 with their corresponding flux plots in Figure 4.4, the later appearance of waves in Figure 4.5c as compared with that of Figure 4.5a corresponds to the diffusion of Ca^{2+} entering the cell through the individual LCCs in order to reach the CRUs elsewhere to begin the process of CICR, since the LCCs are everywhere in the cell as opposed to directly across from the CRUs. In the case of Figure 4.5a, since the LCCs are directly across from the CRUs with greater flux entering the cell from the extracellular space, then CICR is more easily triggered considering the same pump sensitivity.

6 Conclusions

Based on our simulation observations, we have been able to make various conclusions regarding the influence of the elements we implemented in the original mathematical model [10]. Increasing initial SR Ca^{2+} concentration increases probability of calcium waves, though flooding of the cell can occur with a higher SR Ca^{2+} diffusion coefficient and low strength of the SR pump that pulls Ca^{2+} back into the cell. The addition of a buffer into the SR behaved as expected, decreasing the likelihood of wave propagation. Also as expected, we saw an increased probability of wave dynamics and, even more likely, calcium flooding in the cell when the voltage difference across the plasma membrane was included in the model. Overall, our findings aligned with known biological models and principles, giving us a thorough understanding of several factors that influence Ca^{2+} dynamics in cardiac myocytes.

Acknowledgments

These results were obtained as part of the REU Site: Interdisciplinary Program in High Performance Computing (hpcreu.umbc.edu) in the Department of Mathematics and Statistics at the University of Maryland, Baltimore County (UMBC) in Summer 2015. This program is funded by the National Science Foundation (NSF), the National Security Agency (NSA), and the Department of Defense (DOD), with additional support from UMBC, the Department of Mathematics and Statistics, the Center for Interdisciplinary Research and Consulting (CIRC), and the UMBC High Performance Computing Facility (HPCF). HPCF is supported by the U.S. National Science Foundation through the MRI program (grant nos. CNS-0821258 and CNS-1228778) and the SCREMS program (grant no. DMS-0821311), with additional substantial support from UMBC. Co-author Michael McCauley was supported, in part, by the UMBC National Security Agency (NSA) Scholars Program through a contract with the NSA. Graduate assistant Zana Coulibaly was supported during Summer 2015 by UMBC.

References

- [1] Antzelevitch, C., S. Sicouri. (1994). Clinical relevance of cardiac arrhythmias generated by afterdepolarizations, *Journal of the American College of Cardiology*, **23**, 259-277.
- [2] Balke, C.W., L. Goldman. (2003). Excitation contraction coupling in cardiac muscle, *Journal of General Physiology*, **121**, 349-352.
- [3] Cannell, M.B., C.H.T. Kong, M.S. Imtiaz, and D.R. Laver. (2013). Control of sarcoplasmic reticulum Ca^{2+} release by stochastic RyR gating within a 3D model of the cardiac dyad and importance of induction decay for CICR termination, *Biophysical Journal*, **104**, 2149-2159.
- [4] Catterall, W.A. (2011). Voltage-gated calcium channels, *Cold Spring Harbors Perspectives in Biology*, **3**, 1-23.
- [5] Cheng, H., W.J. Lederer, and M.B. Cannell. (1993). Calcium sparks: elementary events underlying excitation-contraction coupling in heart muscle, *Science*, **262**, 740-744.
- [6] Coulibaly, Z., M.K. Gobbert, and B.E. Peercy. (2014). Insight into spontaneous recurrent calcium waves in a 3-D cardiac cell based on analysis of a 1-D deterministic model, *International Journal of Computer Mathematics*, **92**, 591-607.
- [7] Ford, L.E., R.J. Podolsky. (1970). Regenerative calcium release within muscle cells, *Science*, **167**, 58-59.
- [8] Gilabert, J.A. (2012). Calcium signaling, *Advances in Experimental Medicine and Biology*, **740**, 483-498.
- [9] Gobbert, M.K. (2008). Long-time simulations on high resolution meshes to model calcium waves in a heart cell, *SIAM Journal of Scientific Computing*, **30**, 2922-2947.

- [10] Izu, L.T., W.G. Wier, and C.W. Balke. (2001). Evolution of cardiac calcium waves from stochastic calcium sparks, *Biophysical Journal*, **80**, 103-120.
- [11] Lee, Y.S., J.P. Keener. (2008). A calcium-induced calcium release mechanism mediated by calsequestrin, *Journal of Theoretical Biology*, **253**, 668-679.
- [12] Marks, A.R. (2003). Calcium and the heart: a question of life and death, *Journal of Clinical Investigation*, **111**, 597-599.
- [13] Morris, C., H. Lecar (1981). Voltage oscillations in the barnacle giant muscle fiber, *Biophysical Journal*, **35**, 193-213.
- [14] Picht, E., A.V. Zima, T.R. Shannon, A.M. Duncan, L.A. Blatter, and D.M. Bers. (2011). Dynamic calcium movement inside cardiac sarcoplasmic reticulum during release, *Circulation Research*, **108**, 846-856.
- [15] Ramay, H.R., M.S. Jafri, W.J. Lederer, and E.A. Sobie. (2010). Predicting local SR Ca²⁺ dynamics during Ca²⁺ wave propagation in ventricular myocytes, *Biophysical Journal*, **98**, 2515-2523.
- [16] Ringer, S. (1883). A further contribution regarding the influence of the different constituents of the blood on the contraction of the heart, *Journal of Physiology*, **4**, 29-42.
- [17] Shiferaw, Y., G.L Aistrup, and J.A. Wasserstrom. (2012). Intracellular Ca²⁺ waves, afterdepolarizations, and triggered arrhythmias, *Cardiovascular Research*, **95**, 265-268.
- [18] Smith, G., N. MacQuaide. (2008). Cytoplasmic versus intra-SR: the battle of the Ca²⁺ diffusion coefficients in cardiac muscle, *Biophysical Journal*, **95**, 1005-1006.
- [19] Swietach, P., K.W. Spitzer, and R.D. Vaughan-Jones. (2010). Modeling calcium waves in cardiac myocytes: importance of calcium diffusion, *Front Biosci (Landmark Ed)*, **15**, 661-680.
- [20] Swietach, P., K.W. Spitzer, and R.D. Vaughan-Jones. (2008). Ca²⁺-mobility in the sarcoplasmic reticulum of ventricular myocytes is low, *Biophysical Journal*, **95**, 1412-1427.
- [21] Weiss, J.N., A. Garfinkel, H.S. Karagueuzian, P. Chen, and Q. Zhilin. (2010). Early afterdepolarizations and cardiac arrhythmias, *Heart Rhythm Society*, **7**, 1891-1899.